Space Weather

RESEARCH ARTICLE
10.1029/2024SW004189

The Need for a Sub-L1 Space Weather Research Mission: Current Knowledge Gaps on Coronal Mass Ejections

Noé Lugaz[1], Nada Al-Haddad[1], Bin Zhuang[1], Christian Möstl[2], Emma E. Davies[2], Charles J. Farrugia[1], Sahanaj Aktar Banu[1], Eva Weiler[2,3], and Antoinette B. Galvin[1]

[1]University of New Hampshire, Durham, NH, USA, [2]Austrian Space Weather Office, Geosphere Austria, Graz, Austria, [3]Institute of Physics, University of Graz, Graz, Austria

Key Points:

- In-situ measurements of CME magnetic ejecta near 1 au do not vary significantly within $\lesssim 0.3°$
- A sub-L1 research mission is needed to learn about CME evolution and variations on moderate scales and to characterize orbit requirements
- Data from STEREO-A provide a proof-of concept of sub-L1 monitors with lead times of several hours and only a small drop in accuracy

Correspondence to:
N. Lugaz,
noe.lugaz@unh.edu

Citation:
Lugaz, N., Al-Haddad, N., Zhuang, B., Möstl, C., Davies, E. E., Farrugia, C. J., et al. (2025). The need for a sub-L1 space weather research mission: Current knowledge gaps on coronal mass ejections. *Space Weather*, *23*, e2024SW004189. https://doi.org/10.1029/2024SW004189

Received 30 SEP 2024
Accepted 18 JAN 2025

Author Contributions:
Conceptualization: Noé Lugaz, Nada Al-Haddad
Data curation: Noé Lugaz, Bin Zhuang, Sahanaj Aktar Banu, Eva Weiler
Formal analysis: Noé Lugaz
Funding acquisition: Noé Lugaz, Christian Möstl, Antoinette B. Galvin
Investigation: Noé Lugaz
Methodology: Noé Lugaz
Visualization: Noé Lugaz
Writing – original draft: Noé Lugaz
Writing – review & editing: Nada Al-Haddad, Bin Zhuang, Christian Möstl, Emma E. Davies, Charles J. Farrugia

Abstract Over the past decades, missions at the L1 point have been providing solar wind and interplanetary magnetic field measurements that are necessary for forecasting space weather at Earth with high accuracy and a lead time of a few tens of minutes. Improving the lead time, while maintaining a relatively high level of accuracy, can be achieved with missions sunward of L1, so-called sub-L1 monitors. However, too much is unknown to plan for sub-L1 monitors as operational missions: both the orbital requirements of such missions, and the achievable accuracy of forecasts based on their measurements have not been quantitatively defined. We review here some proposed mission concepts and explain the knowledge gaps related to coronal mass ejections (CMEs) that require a space weather research or science mission. We first show how STEREO-A measurements in 2023 can be used as a proof of concept of the use of sub-L1 monitor slightly off the Sun-Earth line to forecast the Dst index. We then highlight that separations of $\lesssim 10°$ are needed to ensure that CMEs measured by a sub-L1 monitor impact Earth. Next, we show that measurements with angular separations of $\lesssim 0.35°$ have negligible errors but separations of a few degrees can result in significant errors in lead time and in the forecasted magnetic field strength of CMEs. We also discuss how CME evolution over the last 0.05–0.2 au before impacting Earth is strongly under-constrained and needs to be better understood before using measurements of sub-L1 monitors for real-time space weather forecasting.

Plain Language Summary Since the late 1990s, spacecraft which are 1% closer to the Sun than Earth have been providing measurements of the solar wind and interplanetary magnetic field to forecast space weather at Earth with a lead time of a few tens of minutes. Improving the lead time can be achieved with missions going closer to the Sun. During 2023, the STEREO-A spacecraft took data about 3%–5% closer to the Sun than Earth. We use that data as proof of concept of such measurements to forecast space weather at Earth. We then discuss how different angular separations, ranging from a fraction of a degree to 15° with the Sun-Earth line may or may not affect the accuracy of the measurements from such platforms. We conclude by pointing out that research missions are needed to fill our understanding gaps before operational missions are possible.

1. Introduction

The launch of the Deep Space Climate Observatory (DSCOVR, see Loto'aniu et al., 2022) in 2015 and the confirmation of the Solar Wind Follow-On (SWFO)-L1 mission to be launched in 2025 (Talaat, 2023) mark a new era for interplanetary (IP) measurements, one where operational missions provide in situ measurements of the solar wind and interplanetary magnetic field (IMF), including coronal mass ejections (CMEs), shocks and stream interaction regions (SIRs). These operational missions at the first Sun-Earth Lagrangian (L1) point complement rather than replace, scientific missions with similar instrumentation such as *Wind* (Wilson et al., 2021) and IMAP (to be launched in 2025, see McComas et al., 2018). The International Sun/Earth Explorer (ISEE)-3 (Farquhar, 2001) was the first spacecraft to go into a Sun-Earth L1 orbit in 1978, staying there for 3.5 years before being re-tasked into a cometary mission as the International Cometary Explorer. The 1990s saw SOHO and ACE (Stone et al., 1998) launched into L1 orbits where they were joined by *Wind* in 2004 (Wilson et al., 2021) after it executed numerous near-Earth orbits and an excursion in the far Earth magnetotail. As such, it took over 35 years between the first scientific and the first operational mission at L1. Similarly, any future operational L4/L5 missions such as Vigil (e.g., see Eastwood et al., 2024) will be launched at least two decades after the launch of the twin Solar-Terrestrial Relations Observatory (STEREO, see Kaiser et al., 2008) in 2006, and 15–20 years after STEREO-A and B first reached the L4 and L5 points.

The instrumentation and overall observatory needed to perform in situ space weather research or operational forecasts in the IP space, including propulsion and telemetry systems, are well understood and of high heritage. In some sense, it builds upon decades of heritage from missions like ISEE-3, Ulysses, ACE, *Wind* and even older missions such as Helios and Interplanetary Monitoring Platform. There is also a general consensus that in situ measurements upstream (i.e., sunward) of L1, hereafter referred to as sub-L1 measurements, shall provide actionable space weather forecasts (see for example discussion in Morley, 2020). In light of this, there have been some discussions of designing and developing sub-L1 operational monitors based on current knowledge and understanding of space weather forecasting. In this article, we argue that current scientific knowledge is not advanced enough to bypass a science phase focusing on space weather research. We also discuss how, while STEREO provided some of the required measurements to prove the science benefits of sub-L1 monitors, it occurred over a too short time period to fully constrain the requirements of an operational sub-L1 monitor. This is for two main reasons. First, the optimal orbit for such a mission cannot be determined from our current scientific knowledge of IP transients (CMEs and shocks). This is due to the relative paucity of multi-spacecraft measurements of such transients for spacecraft separated by 0.5–10°, that is, separations likely to be achieved by operational missions. Second, the way the solar wind, IMF and transients evolve as they propagate on these moderate radial separations of 0.05–0.25 au is also currently unknown. The few examples we have, typically from missions in transit to their final orbit, reveal that there can be changes that would affect the accuracy of forecast based on these sub-L1 measurements. Recent measurements by STEREO-A as it crossed the Sun-Earth line sunward of L1 in August 2023 have revealed that further research is required. As discussed below, we show that the knowledge gained from STEREO-A's recent measurements can be used to constrain the orbital requirements for a space weather research mission, which could also serve as a pathfinder for a sub-L1 space weather monitor and provide beacon data that can be used for space weather forecasting.

Lindsay et al. (1999) used data from Pioneer Venus Orbiter when the spacecraft was ±10° from the Sun-Earth line and near the ecliptic over a 27-day period in June 1980 to forecast the Dst storm time index using measurements from 0.72 au. This included two SIRs and two CMEs. The peak of the strongest geomagnetic storm caused by a CME was well predicted using the PVO measurements and the formula from Burton et al. (1975). The authors also used Helios data from ∼10° east and ∼5° north of the ecliptic to forecast Dst over a 54-day period, including three geomagnetic storms with a peak Dst below −80 nT, two of which were well predicted by the Helios data. More recently, Venus data combined with remote observations were used to hindcast the CME impact at Earth (Kubicka et al., 2016). Laker et al. (2024) recently showcased the capabilities of Solar Orbiter, when it is close to the Sun-Earth line and sunward of L1, to serve as an upstream solar wind monitor, during a period in March 2022 when it was around 0.44–0.48 au. The authors successfully hindcasted the arrival time of two CME events before they reached Earth, reducing the uncertainty in arrival time from 10.4 to 2.5 hr in one of the two case studies. The data taken by STEREO-A around the time that it passed sunward of the L1 point in August 2023 can be used as a further proof of concept for the usability of such sub-L1 measurements to forecast space weather at Earth, as is done in Section 2.

Two major gaps in our understanding of CMEs limit our ability to move toward an operational sub-L1 monitoring platform: (a) how CME properties vary on moderate angular scales: 0.2°–15° and (b) how CME properties vary as they propagate over moderate distances: 0.05–0.2 au. These two issues were recently highlighted by the case of the May 2024 superstorm associated with multiple successive and interacting CMEs (Liu et al., 2024) where STEREO-A observed a different resulting complex ejecta than spacecraft at L1 although they were only separated by 12° in longitude and 0.04 au in heliocentric distance. However, these STEREO-A measurements can still be used to forecast Dst with a lead time of ∼2.5 hr ahead of L1, with good accuracy (Weiler et al., 2024). We further discuss the consequences of these two knowledge gaps on potential space weather forecasting with sub-L1 monitors, using L1 measurements from ACE and *Wind* and measurements from L1 and STEREO-A to highlight the issue of the variability of CME properties on moderate angular scales and recent studies to highlight the variations of CME properties over moderate distances.

The rest of the article is organized as follows. In Section 2, we discuss the instrumentation for IP missions, the rationale behind sub-L1 operational measurements, the potential orbits for sub-L1 missions, and present a proof of concept of such missions with STEREO-A measurements in 2023. In Section 3, we first discuss how variations between spacecraft at L1 or between L1 and Earth are usually negligible for CMEs. We then show some examples where small angular separations between two spacecraft in the IP space result in large differences in CME measurements. In Section 4, we present examples where the evolution of CMEs over distances of 0.1–0.2 au

differs significantly from the average trend obtained over decades of measurements. We discuss how such a behavior may affect the accuracy of forecasts based on sub-L1 measurements. In Section 5, we argue that science or space weather research missions are first needed to solve these issues before launching operational missions. We also discuss some of the current issues with hybrid approaches, and present our conclusions. In Section 6, we make some recommendations regarding sub-L1 missions.

2. Sub-L1 Missions: Rationale, and Instrumentation

2.1. Rationale and Instrumentation

Over the past two decades, significant progress has been made in forecasting CME speed, hit/miss and arrival times from coronagraphic observations (e.g., see Kay et al., 2024; Riley et al., 2018; Vourlidas et al., 2023), although these often rely on having a second (or third) viewpoint provided by STEREO. CME deflection after their initiation (Kay et al., 2013; Wang et al., 2004, 2006; Zhuang et al., 2017) and so-called stealth CMEs (Howard & Harrison, 2013; Nitta et al., 2021) are two of the key factors that affect the hit/miss predictions. Overall, typical error bars are on the order of ± 10–12 hr and there are still events which are missed or forecast incorrectly (False Positives and False Negatives), and typical lead times are several tens of hours for a typical CME speed (Kay et al., 2024). These values are similar for both empirical and numerical modeling, such as those provided by ENLIL (Odstrcil et al., 2003). Machine-learning approaches have been recently reported to yield more accurate predictions (Liu et al., 2018; Yang et al., 2023) but they need to be further validated in operational-like settings. In addition, there has been progress in making at least hindcast of the CME orientation (the so-called B_z forecasting), also from coronagraphic observations, often combined with magnetogram and EUV observations, and semi-empirical models (e.g., see Kay et al., 2022; Möstl et al., 2018; Palmerio et al., 2018; Sarkar et al., 2024; Savani et al., 2013). Such models have not been validated as exhaustively as forecasting models of the CME speed and arrival time. One of the hardest parameters to forecast is the magnitude of the magnetic field inside CMEs. Savani et al. (2015) used the average value of all CMEs, whereas 3DCORE (Möstl et al., 2018; Rüdisser et al., 2024; Weiss et al., 2021) uses a power law for the CME evolution (Leitner et al., 2007) and fixes the field magnitude with available in situ magnetic field data. OSPREI and FIDO use a scaling of the ambient magnetic field to determine the initial magnetic field inside the ME (Kay et al., 2022). Numerical simulations without internal magnetic field inside the CME, such as ENLIL (Odstrcil & Pizzo, 2009), are not able to reproduce the magnetic field magnitude, whereas others, such as the SWMF (Tóth et al., 2012) and EUHFORIA (Poedts et al., 2020; Pomoell & Poedts, 2018) have not been fully validated in real-time operational settings.

In situ measurements, including from a sub-L1 mission have two main advantages and one main drawback as compared to these current approaches: (a) they provide full plasma and magnetic field measurements, and are currently our only way to measure the CME magnetic field (at least beyond ∼5 $R_\odot$), not just its orientation, although the magnetic field can be modeled or inferred through various techniques, (b) they are accurate, providing what is considered as the "ground truth" to which other methods are compared. However, (c) their lead time is currently only 15–60 min for measurements at L1. Taking sub-L1 measurements, therefore, seems like a natural solution for the only drawback without affecting the two main advantages (More discussion on this below.) We note that, just like L1 measurements, sub-L1 measurements would provide information about the local properties of the solar wind and transients therein. As such, their use for forecasting the conditions just upstream of Earth's bow shock is only appropriate as long as these "local" measurements do not vary greatly over the temporal and spatial scales separating the observing platform and Earth. The effect of the uncertainty of L1 measurements on the expected geo-effectiveness was quantified through a series of ensemble simulations in Morley et al. (2018), for the 2010 April 5 CME. The authors found for example, that the uncertainty in L1 measurements could result in variations of ±4 nT of the mean absolute error on the simulated Sym-H index (the 1-min equivalent to Dst).

Based on a typical shock speed of 500 km s^{-1} (Kilpua et al., 2015; Salman et al., 2021), each 0.01 au upstream of L1 corresponds to an additional 50 min of advanced warning. For a fast event with speed at 1 au of 800 km s^{-1} (corresponding to geomagnetic superstorms like the March 2001, May 2024 or the 2003 Halloween events), each 0.01 au corresponds to an additional 30 min. For a potentially extreme event with a speed of 2,000 km s^{-1} (similar to the 2012 July 23 CME, see Liu et al., 2014), each 0.01 au only provides an additional 12.5 min of warning. Overall, measurements at 0.88 au would provide a 12-hr warning for a typical CME, while measurements at 0.8 au would be necessary to provide a 12-hr warning for fast events and a 4-hr warning for the most extreme events. It is

likely that sub-L1 in situ measurements would be used in conjunction with remote observations to constrain models and ensemble forecasts or through data assimilation in numerical simulations. This has been the case for measurements at Venus and with Solar Orbiter, additionally using STEREO remote observations (Kubicka et al., 2016; Laker et al., 2024).

Any sub-L1 mission, whether research or operational, is likely to rely on a relatively simple, high-technology readiness level (technology readiness level) instrumentation to measure plasma and magnetic field without redundancies. The measurement requirements are driven by the extreme velocity, temperature and density (both high and low) measured often within CMEs (for velocity, density and magnetic field), as well as associated solar energetic particle measurements. It is likely to be similar to SWFO-L1 instrument requirements at minimum and resemble the in situ suites of IMAP or STEREO for their most complex payload. At minimum, this would be (a) solar wind proton moments for speeds of 250–2,000 km s^{-1}, densities of 0.1–150 cm^{-3}, and temperatures from 10^3 to 10^6 K, (b) magnetic field with a range in each component of ±150 nT, (c) energetic ions and electrons with energies from 50 keV to at least 10 MeV for ions and 1 MeV for electrons, corresponding typically to energies associated with SIRs or ions locally accelerated at the shock (energetic storm particle events). The baseline in situ instrumentation package may weigh less than 10 kg and use less than 10 W of power, based on current heritage (e.g., see Lugaz, Lee, et al., 2024). A sub-L1 platform does not necessarily provide a better location for remote-sensing instrumentation, such as coronagraphs, EUV or X-ray instruments as compared to L1. It would improve the spatial resolution of these remote measurements only incrementally, as it depends on the distance to the Sun, which only decreases by 2%–20% as compared to L1. However, the associated telemetry depends on the distance to Earth which increases by a factor of 2–20 as compared to L1. In addition, those instruments typically have more stringent pointing requirements than in situ instruments. As such, it is likely that a sub-L1 monitor would have only an in situ instrumentation payload. This would enable the bus to be spin-stabilized, similar to IMAP, ACE and *Wind*. A spin-axis in the ecliptic like IMAP and ACE would allow for easy real-time telemetry to Earth for some of the potential orbits for a sub-L1 monitor. Missions that venture significantly beyond the Sun-Earth line, such as Vigil at L5, do provide a better vantage point as compared to L1 to observe a significant portion of the solar disk, corona and heliosphere, making them ideal platforms to combine remote and in situ observations.

2.2. Proof of Concept: STEREO-A Measurements in 2023

STEREO-A orbits the Sun at a heliocentric distance of ∼0.95–0.97 au and is therefore 0.01–0.06 au upstream of Earth (depending on Earth's exact heliocentric distance). During 2023, STEREO-A crossed the Sun-Earth line going from ∼13.8° east to 7.0° west of it. This occurred during a period of high solar activity with around 30 CMEs measured at L1 as reported in various databases (Möstl et al., 2020; Richardson & Cane, 2010). This allows for a unique proof of concept of sub-L1 monitors. Detailed analyses of specific geomagnetic storms and CME events during this time period are ongoing. Here, we present a high-level overview of the STEREO-A measurements and their usage to forecast the disturbed storm time (Dst) index.

We focus on two time periods, before and after STEREO-A crossed the Sun-Earth line on 2023 August 13. From 2023 March 20 to August 6 (east period), STEREO-A was 0.5–12° east of the Sun-Earth line and on average 0.051 au upstream of Earth. During this time period, there were six moderate geomagnetic storms (peak Dst between −99 nT and −50 nT), and two intense ones (peak Dst below −100 nT). From 2023 August 21 to December 10 (west period), STEREO-A was 0.8–6.6° west of the Sun-Earth line and on average 0.037 au upstream of Earth. During this time period, there were seven moderate geomagnetic storms, and three intense ones. We note that, while STEREO-A measures corotating structures before they impact Earth during the east period, this is also the case at the beginning of the west period (up to separations of ∼2.5) because STEREO-A is upstream of Earth.

We use the STEREO-A 1-min solar wind and IMF measurements to calculate the "predicted" (in hindcast) Dst using the formula from O'Brien and McPherron (2000). We use science-level data, rather than beacon data which is available in real-time, from STEREO-A as the focus here is to provide a proof of concept. We use a single time-shift to shift the STEREO-A measurements to the OMNI location ($t_{OMNI} - t_{STEREOA}$). This time-shift is calculated to maximize the correlation between the 1-min OMNI data and STEREO-A measurements of the strength of the magnetic field. Clearly, the time-shift could be optimized for smaller time periods or using a propagation tool such as done to create the OMNI data from L1 measurements, but this is left for future work. The best time-shift is 309 min for the east period, corresponding to a solar wind speed of about 401 km s^{-1} assuming radial propagation

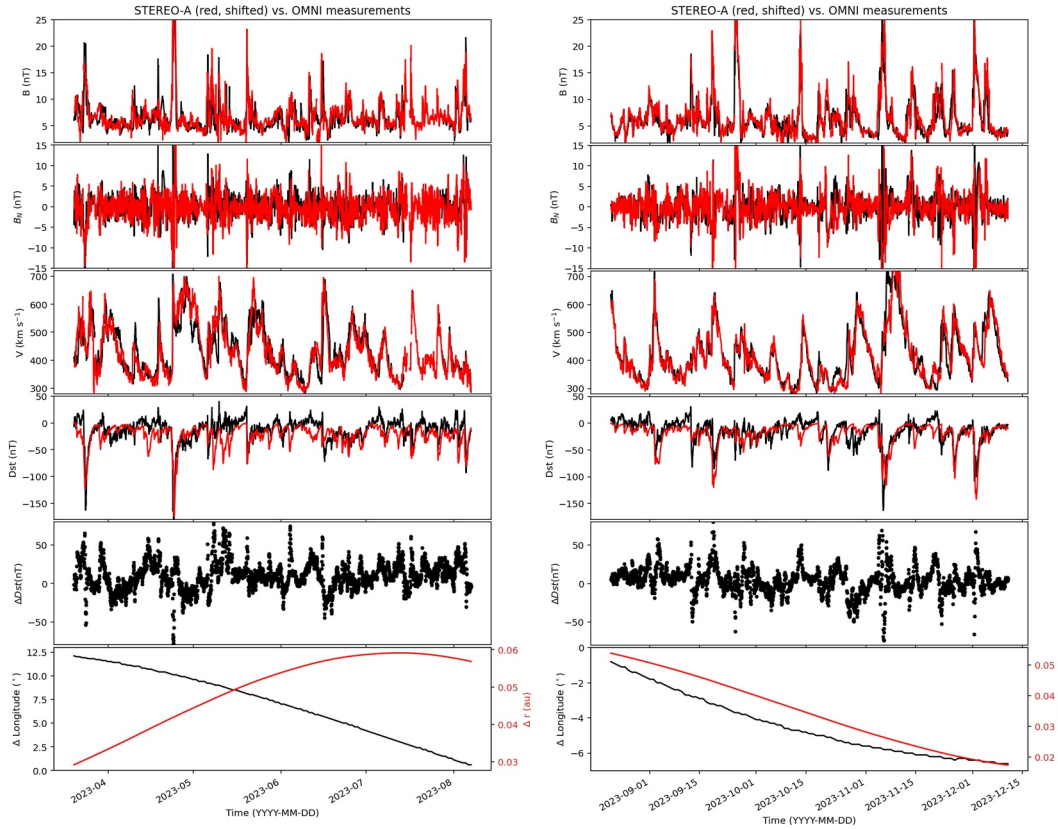

Figure 1. Time-shifted STEREO-A (red) versus OMNI (black) data for two time periods in 2023 where STEREO-A can be used as an upstream monitor. The panels show from top to bottom, the interplanetary magnetic field (IMF) strength, the north-south component of the IMF, the solar wind speed, the measured and predicted Dst indices, the difference between them and the longitudinal separation (black) and separation in heliocentric distances (red) between STEREO-A and Earth. The left and right panels show the time periods when STEREO-A was east and west of the Sun-Earth line, respectively.

and no corotation effects. It is 197 min for the west period, corresponding to a speed of about 460 km s^{-1}. The average solar wind speed for these two time periods is 430–440 km s^{-1}, close to the values obtained with the simple approximation. The fact that this is close to the assumption of radial propagation implies that the main drivers of large magnetic field during these time periods are CMEs not corotating interaction regions, which would have a very different time-shift for the east and west periods. The fact that the timeshift for the west period is smaller than for the east period is primarily due to the smaller average difference in heliocentric distance with Earth but there is a likely contribution from the corotating effect. Assuming the same speed of 430 km s^{-1} for both east and west periods, one can estimate the difference between the two time-shifts as 25 min which is not due to the different radial distances at this time.

Figure 1 shows the results of this procedure with the predicted Dst from STEREO-A measurements in red in the penultimate panel as compared to the Dst index. No correction is used for the dynamic pressure effects. We directly use the north-south component of the magnetic field in GSE/RTN coordinates without transforming into GSM coordinates on which the formula of O'Brien and McPherron (2000) is based. The average root mean square error (RMSE) for the Dst prediction from STEREO-A data is 20.8 nT for the east period and 18.0 nT for the west period. The value using the OMNI data to forecast Dst is 14.1 and 13.9 nT during both periods. Most geomagnetic storms are captured with a relatively small number of false positives, that is, storms that were predicted but not observed. During the east period, there are false positives on April 14–15, May 7–15 (three peaks) and August 2 (peak Dst reached −45 nT for a prediction of −75 nT), as well as an underestimation of the May 6 and June 16–17 moderate geomagnetic storms. During the west period, there are underestimations on September 12 (partial data gap in STEREO-A measurements), as well as misses of the moderate geomagnetic storms in October 26–29 (two peaks) and November 21–23. Eight of the nine largest geomagnetic storms (Dst below −75 nT) are accurately

forecast (the exception is the September 12 one with the data gap): March 23–24, April 23–24, August 5, September 18–19, October 21, November 5–6, November 25, December 1–2.

To first order, STEREO-A measurements during 2023 appear appropriate to forecast the Dst values at Earth and provide a lead time of 3–5 hr, a significant improvement over data from L1, while maintaining a relatively high accuracy (30%–50% lower than using L1 measurements based on the RMSE). We note that the largest errors in the Dst index as shown in the penultimate panel of Figure 1 appear as a quick succession of large negative and positive errors, which is likely to be associated with small differences in the arrival times of the structures from that obtained from the single time-shift. Further studies are needed to determine whether and how such sub-L1 measurements can be used in a more optimal way to improve the forecast of geomagnetic activity.

We finish this section with three additional remarks. First, there is no obvious trend of the Dst error with the longitudinal separation between STEREO-A and Earth. This might be due to the fact that individual CME events are the main causes of the Dst error and occur randomly within the two time periods. This differs from results found based on data during the early years of STEREO (Bailey et al., 2020; Chi et al., 2022) during the solar minimum of 2007 when geomagnetic activity was driven by corotating structures and the accuracy of prediction showed a clear dependence on the longitudinal and latitudinal separations between STEREO and Earth. Second, the difference in the accuracy of the forecast between the east and west time periods is relatively small. The forecast during the west period at a time when STEREO-A was closer to Earth both in heliocentric distance and longitudinally has an RMSE ∼30% larger than that obtained from OMNI data as compared to ∼48% for the east period. More detailed analyses of the individual storms in 2023 are needed to determine the influence on the accuracy of the heliocentric distance, angular separations and east/west position with respect to the Sun-Earth line. Third, even for these angular separations of 0.5–12°, STEREO-A measurements do provide "adequate" (to be better quantified) way to forecast geomagnetic activity with improved lead times, showcasing the possibility of using sub-L1 monitors away from the Sun-Earth line. In the following section, we further discuss the impact of the longitudinal separation between two spacecraft on the consistency of solar wind and IMF measurements during CME events.

3. Effect of the Angular Separations Between Spacecraft Near 1 AU on CME Measurements

3.1. Occurrence of Two-Spacecraft Measurements Based on Longitudinal Separations

Before quantifying the impact of small-to-moderate angular separations on CME properties, we can first discuss the simplest criterion for the usefulness of such measurements, that is, whether the same CME is measured in situ for two spacecraft separated by a given separation. Good and Forsyth (2016) used planetary missions in the innermost heliosphere (Venus Express and MESSENGER) combined with measurements from near 1 au with STEREO and L1 monitors to determine how often the same CME is measured by two spacecraft separated by some angle in the ecliptic plane. They found that seven out of 40 (17.5%) MEs (the magnetically dominated part of the CMEs) are measured by two spacecraft separated by 30–45°, but 20 out of 42 (47.5%) for separations of 15–30° and 33 out of 41 (80%) for separations of less than 15°. Based on our own analysis of these events (e.g., see Salman et al., 2020), we consider that these numbers are an upper limit, which arises from the fact that there are no plasma measurements for the innermost spacecraft (MESSENGER and Venus Express) and that the CME propagates for 1–3 days between the two spacecraft, which may result in interaction and deflection. Overall, this indicates that separations of less than ∼22.5° (taking the middle of the 15–30° bin) are required to ensure that the majority of MEs are measured by two spacecraft.

Lugaz, Zhuang, et al. (2024) performed an analysis of MEs measured in situ by STEREO-A and *Wind* from 2020 October to 2022 August and found that only five out of 35 events (14%) were measured by the two spacecraft for separations of 20–60°. The data over 2023–2024 is currently being analyzed but confirms that, at separations greater than 15°, fewer than half of the events are measured by two spacecraft at nearly the same heliocentric distance.

Kilpua et al. (2011) reviewed the multi-spacecraft measurements of CMEs early in the STEREO mission (2006–2007). Limiting ourselves to maximum separations of 20° between one STEREO spacecraft and L1, there were 7 two-spacecraft measurements between L1 and STEREO and 4 CMEs which were missed by at least one spacecraft. For the 2007 May 21 and 23 events, we count these at both two-spacecraft measurements as well as

single spacecraft measurements since only one of the two STEREO spacecraft measured the CME also measured at L1 (STEREO-A on May 21, STEREO-B on May 23). The 2007 August 25 CME was only measured at STEREO-A (separation of 15°) and the 2007 October 23 CME was only measured at STEREO-B (separation of 18°).

Overall, this provides important criteria for any sub-L1 mission design to have a maximum longitudinal separation with the Sun-Earth line of $\lesssim$15° to ensure that ∼80% of CME hits are correctly forecasted. The two time periods shown in Figure 1 correspond to angular separations smaller than this threshold.

3.2. Effect of Small Angular Separations: Past Work

Koval and Szabo (2010), Lugaz et al. (2018), and Ala-Lahti et al. (2020) used data from *Wind* prograde orbits in 2000–2002 that reached ∼0.75° from the Sun-Earth line to investigate the variations of the properties of IP shocks, MEs and CME sheaths on small angular separations. Significant differences can exist for shocks and sheath regions at those separations. For example, at 0.7° the correlation between the variations of B_z at ACE and *Wind* is only about 0.3 inside a CME sheath region, using 5-min averages (Ala-Lahti et al., 2020). In contrast, inside MEs, the correlation at these separations is typically greater than 0.8 (Lugaz et al., 2018).

There has recently been significant discussion about the variations of solar wind and IMF structures near Earth on the so-called "mesoscales." Different definitions are used for these mesoscales but it is often referred to as 100's of R_E, that is, 0.25–2° (100–800 R_E). The IMF clock angle measured at ACE and *Wind* sometimes differ by 90°–180° (see specific example of Borovsky, 2018, for separations of 0.3°). Walsh et al. (2019) also compared OMNI and THEMIS data (when in the dayside magnetosheath) to quantify this effect. Their Figure 1 shows an example of a 1-hr period when B_z was about −2 nT at ACE but +2 nT at *Wind*. They also found that the difference in IMF clock angle between L1 and THEMIS had a standard deviation of almost 40°, with the two having the same sign of B_z only 65% of the time. This has led to discussions that L1 monitors themselves are not optimal to forecast structures that impact Earth's magnetopause due to their orbits around L1 that may reach ±0.2° from the Sun-Earth line, combined with the modifications associated with the bow shock and draping in the magnetosheath. Morley et al. (2018) quantified, for one CME event, the effect of the uncertainty of the L1 measurements on the resulting simulated Sym-H index and found that using an ensemble mean is a more accurate predictor of Sym-H than using the L1 measurements directly. This highlights that some of these variations on small-scales may have noticeable effects on the accuracy of the forecasted geo-effectiveness.

3.3. Effect of Small Angular Separations: ACE Versus *Wind*

To quantify the differences in ME properties over small angular separations, we analyze the difference during ME passage as measured by ACE and *Wind* during their "normal" orbits from 2004 onwards. ACE and *Wind* are on different 178-day orbits around L1 with *Wind* on a wider orbit that reaches up to 100 R_E from the Sun-Earth line while ACE stays within ∼40 R_E. As such, the maximum separation is about 140 R_E or 9×10^5 km (i.e., about 0.35°). Their separations change by less than 5 R_E per day, the typical duration of an ME. In 2000–2004, *Wind* performed a number of orbital maneuvers, including around the Sun-Earth L2 point before coming back to an orbit around L1 in mid-2004, where it has stayed since. We have analyzed *Wind* and ACE measurements from 100 MEs between mid-2004 and the end of 2013, which covers the descending phase of solar cycle 23, the solar minimum and the ascending phase and first peak of solar cycle 24. We used the CME database from Nieves-Chinchilla et al. (2018) for *Wind* and from Richardson and Cane (2010) for ACE. We only consider events listed in both databases, which excludes about 50 CMEs measured at *Wind* and 80 measured at ACE. It is almost certain that all CMEs are measured by both spacecraft but this reflects differences in the selection criteria, which we did not attempt to resolve.

For each ME, we analyze the magnetic field measurements with the following procedure: (a) we resample the data into 1-min cadence, (b) we find the time shift between ACE and *Wind* that maximizes the correlation between the B_z component of the magnetic field at the two spacecraft, (c) we shift the *Wind* data and resample data from both spacecraft to 5-min resolution, (d) we plot and fit the data. We end up with 26,971 samples, corresponding to an average of 22.5 hr per ME. The sheath region is not included but disturbed CME wakes (after the end of the ME but before the solar wind can be considered "steady") are often included to see how the difference in the measurements at *Wind* and ACE vary there. Figure 2 shows the plot for the magnitude of B as well as B_z. The best-fit lines in red are B_{Wind} (nT) = 0.996 B_{ACE} (nT) + 0.020 nT and Bz_{Wind} (nT) = 0.974 Bz_{ACE} (nT) − 0.059 nT with r-

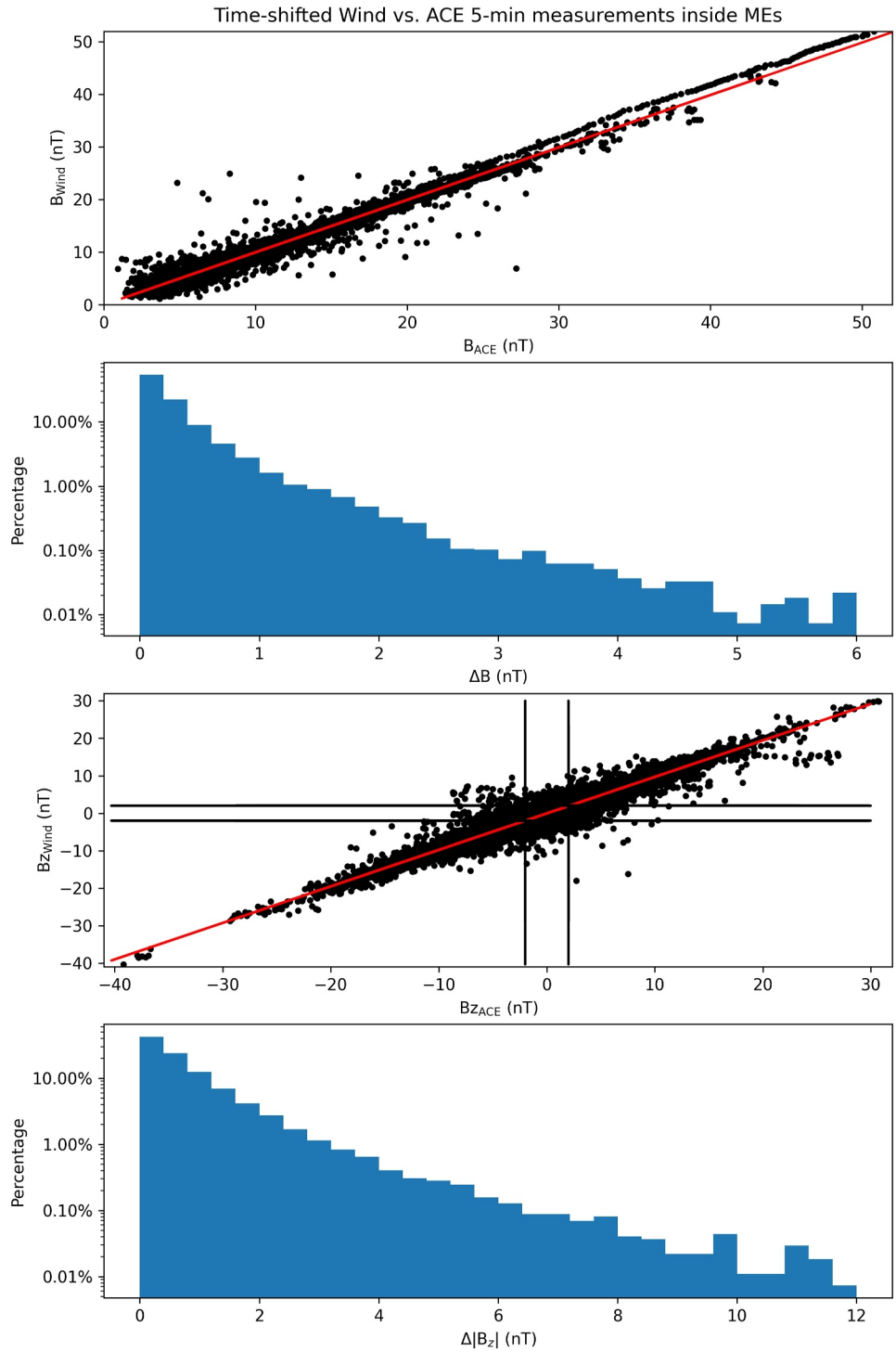

Figure 2. Time-shifted *Wind* versus ACE magnetic field strength (first and second panels) and B_z (third and fourth panels) inside magnetic ejecta and their wakes. 5-minute averages are used. The red lines in the first and third panel show the linear best-fit to the data. The vertical and horizontal black lines in the third panel show the values of ±2 nT. The histograms show the percentage of the data in each of the 30 bins in logarithmic scale. See details in the text about the procedure.

values of 0.991 and 0.978, respectively. This figure can be compared to the ones from Walsh et al. (2019) or the discussion from Borovsky (2018), showing how consistent L1 measurements are between two spacecraft. There are 533 samples (<2% of the total) where B_z at ACE and *Wind* have opposite signs and their product is greater than

1. This is relatively well distributed through the various MEs with a median of 3 per ME and standard deviation of 6.9. For 190 samples (~ 0.7%), B_z at ACE and *Wind* have opposite signs and their product is greater than 4. This is at least one order of magnitude fewer than the 35% of samples with different signs for B_z at *Wind* and THEMIS as reported by Walsh et al. (2019).

The histogram distribution for B shows that more than 50% (resp. 75%) of the points are for a difference in magnitude of less than 0.2 nT (resp. 0.4 nT). The one for B_z shows that more than 40% (resp. 60%) of the points are for an absolute difference of 0.4 nT (resp. 0.8 nT) for B_z. With the number of samples, values at 0.01% correspond to two 5-min samples within our data set. The measurements between ACE and *Wind* differ (calculated as the root mean squared error –RMSE) by 0.478 ± 0.403 nT for $|B|$ and by 1.22 ± 0.658 nT for B_z. Here, we report the medians of the RMSE, but the averages are similar at 0.570 and 1.29 nT, respectively. The large difference in the magnitude of the RMSE for B_z as compared to B can be understood by the range of values reached by these two quantities. $|B|$ typically varies from $B_{max}/2$ to B_{max} where the maximum magnetic field inside a ME is about 12–16 nT for median events (Jian et al., 2018; Regnault et al., 2020), whereas B_z varies from $-B_{zmax}$ to $+B_{zmax}$ where B_{zmax} is typically 6–8 nT. The average value of $|B|$ in our sample, is 9.9 nT (similar to the average value of the magnetic field inside CME at 1 au of 10.1 nT from Richardson & Cane, 2010). As such, the RMSE difference between ACE and *Wind* of 0.478 nT corresponds to about 5% uncertainty in the value of $|B|$.

We next show three example MEs in Figures 3–5 to highlight the limitations of the statistical results and the cause of the difference between ACE and *Wind* measurements. We first show the 2005 July 10–12 ME (Figure 3), which is a relatively long and complex event which has RMSEs very close to the median of our sample: 0.454 nT of RMSE difference for B between ACE and *Wind* and 1.28 nT difference for B_z. At the time of the ME, ACE and *Wind* were separated by about 55 R_E (~3.5×10^5 km) in the GSE y-direction and *Wind* was about 30 R_E upstream of ACE in the GSE x-direction. The panels show the magnetic field strength and component with *Wind* time-shifted in red, the radial velocity from ACE, and $|\Delta B|$ as well as $|\Delta B_z|$ (calculated as RMSE). The best time shift is 11 min, which is consistent with a propagation speed of about 300 km s^{-1} from *Wind* to ACE, a bit lower than the actual CME speed measured here. It is relatively clear that the time-shifting over a period of nearly two days is a source of error, with small time shifts (e.g., around 18 UT on July 11 for B_z) resulting in two datapoints (10 min) with $\Delta B_z > 4$ nT. One can also notice that there is a compression at the end of the event due to the faster solar wind speed and that it does not occur at the same time shift for *Wind* and ACE, resulting in two datapoints (10 min) with $\Delta B > 2$ nT. However, it remains clear that for these values of RMSE (which correspond to the median of our sample), the two profiles are visually extremely similar. We note also that there are only three datapoints when B_z has the opposite sign at ACE and *Wind* and B_z is greater than 1 nT. The largest value of these three datapoints is $B_z = -2.43$ nT at ACE and $B_z = 1.27$ nT at *Wind*. Such differences, lasting only 5 min are unlikely to have significant consequences on space weather forecasting.

The second example is the 2012 June 17 ME (Figure 4), which is a strong event which occurred at a time when the ACE-*Wind* non-radial separation was close to its maximum (~141 R_E or 9×10^5 km). The separation along the GSE x-direction was very small at about 9 R_E. The time shift to maximize the correlation in B_z between ACE and *Wind* is 1 minute. The RMSE for B is 1.96 nT and it is 3.78 nT for B_z, which is the largest RMSE for B_z for any of the 100 CMEs we investigate. There are 14 datapoints for which B_z has the opposite sign at ACE and *Wind* and B_z is greater than 1 nT. The longest continuous period when this condition is verified lasts 30 min starting at 13:35 UT on June 17, when B_z at ACE was ~− 7 nT and it was ~+ 4 nT at *Wind*. Based on the speed of the CME, this feature is about 7.5×10^5 km in radial size or comparable to the ACE-*Wind* non-radial separation. As seen from the plot, it corresponds to a period when there was a relatively sharp discontinuity in B_z at ACE but not at *Wind*. There are also large differences in the B_z positive period in the front of the ME, which may correspond to sub-optimal time shifting for this feature. It is clear from the plot that the largest differences occur toward the boundaries of the selected time period, which may indicate that a single time-shift is not optimal. At ACE and *Wind*, the end time of the ME is selected in the existing database to be around 12 UT. The period with some of the largest differences between ACE and *Wind* measurements therefore correspond to the wake of the CME, which we include here because it corresponds to large values of the magnetic field.

The third example is the 2012 January 21 ME (Figure 5), which is the first half of a two-CME event with a shock inside the ME. Shocks inside ME are a relatively frequent occurrence (Lugaz et al., 2015) and have been shown to result in stronger geo-effects (Lugaz et al., 2016). However, identifying the end of the ME inside which the shock propagates is typically hard. The ACE-*Wind* non-radial separation during this time period was ~75 R_E (or

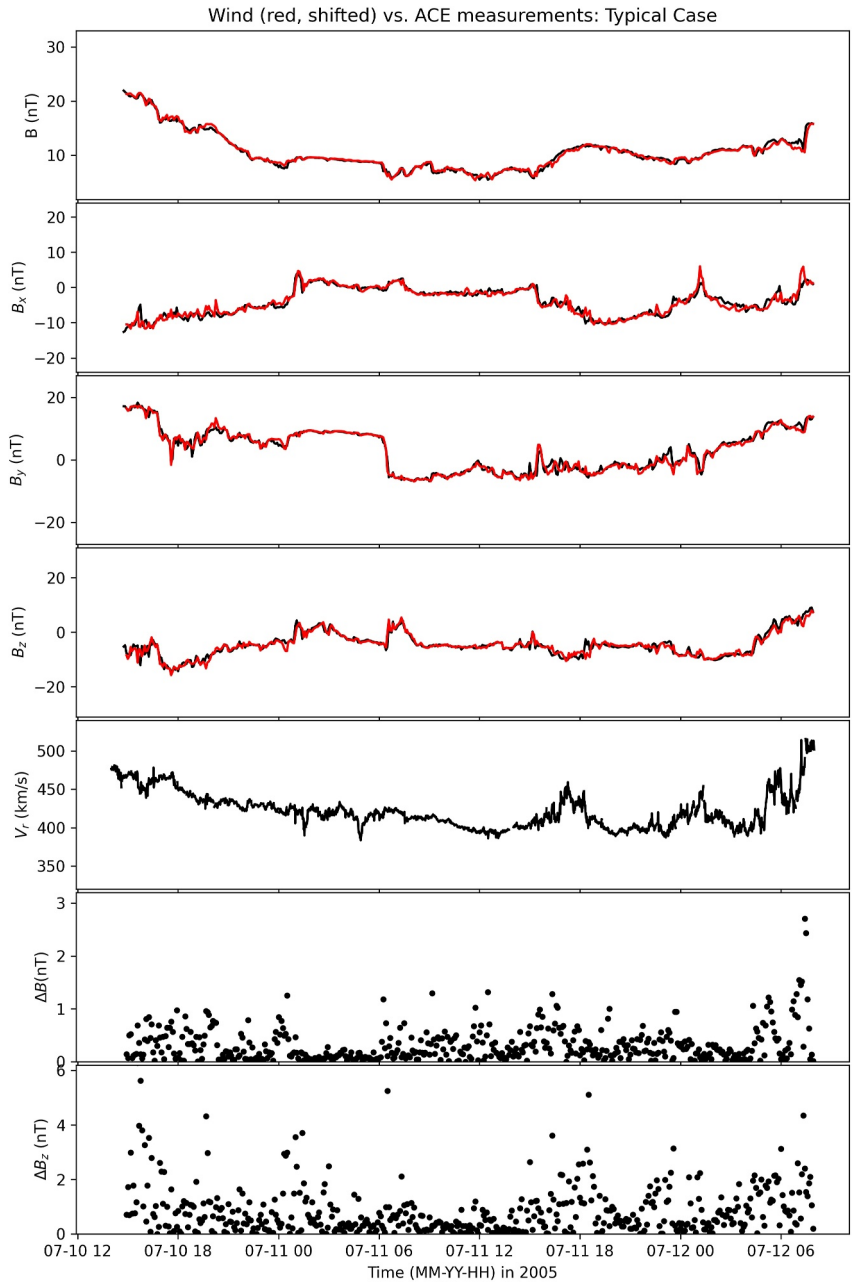

Figure 3. Time-shifted *Wind* (red) versus ACE (black) measurements for the 2005 July 10–12 coronal mass ejection. The panel shows from top to bottom the total magnetic field, the x, y, z components in GSE coordinates, the radial speed, the point-by-point differences in B and B_z. *Wind* and ACE were separated by 55 R_E along the y-direction.

4.8×10^5 km) and ACE was also about 43 R_E upstream of *Wind*. The best time shift is 14 min, consistent with a solar wind speed of about 330 km s^{-1}. The RMSE for B is 0.972 nT and it is 1.73 nT for B_z. There are four datapoints for which B_z has opposite sign at ACE and *Wind* and B_z is greater than 1 nT. The largest difference occurs at 7:30 UT when ACE measures 5.1 nT and *Wind* −8.6 nT. This occurs at the very end of the ME when the field is relatively quickly fluctuating and rotates from ∼10 to ∼− 25 nT over 10 min at both ACE and *Wind* and this is the middle datapoint of this rotation. There are also large differences (up to 5–10 nT) in B_z within the ME but they have the same sign. The largest differences occur in the shocked portion of the ME. This is expected since this time period combines characteristics of sheath regions and ME and sheath regions have smaller correlation lengths than MEs (Ala-Lahti et al., 2020).

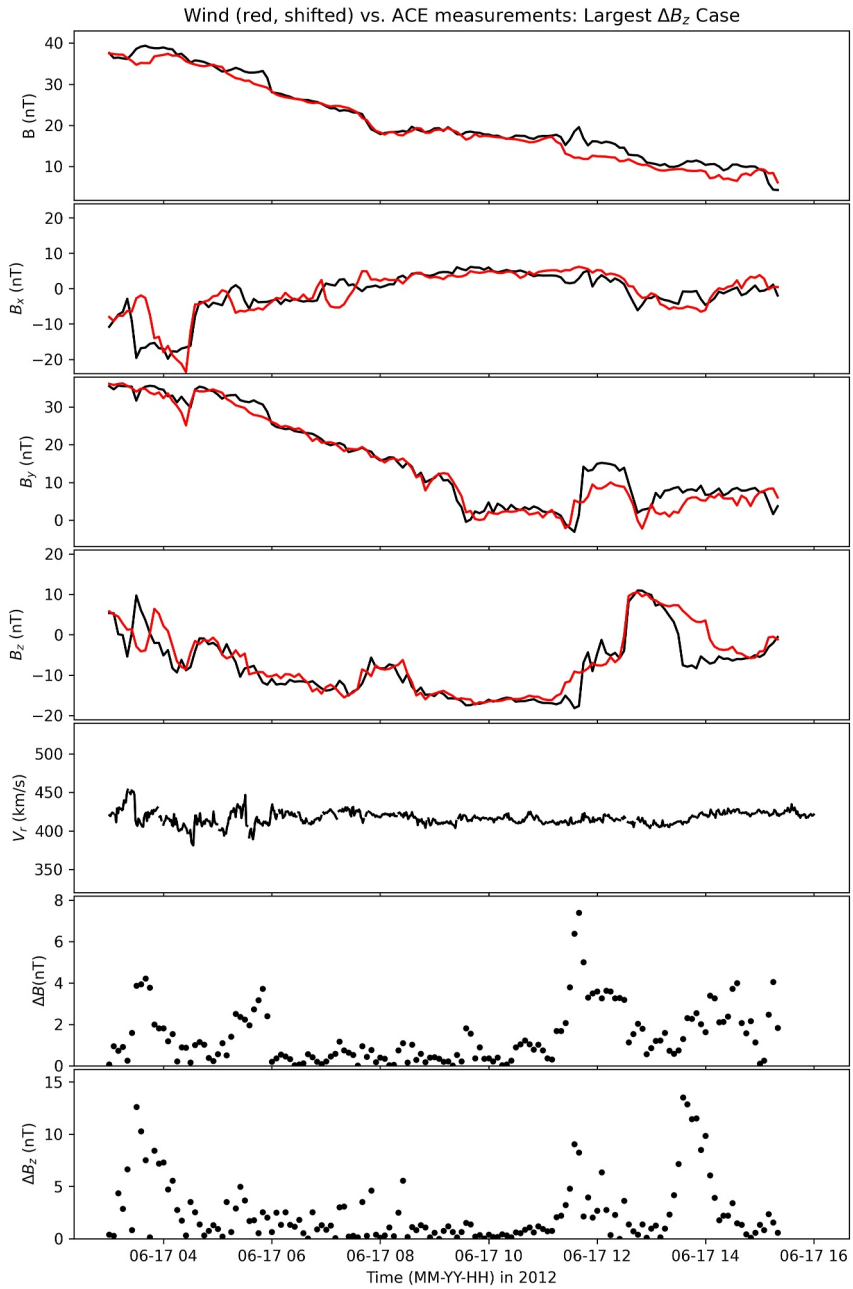

Figure 4. Time-shifted *Wind* (red) versus ACE (black) measurements for the 2012 June 17 coronal mass ejection in the same format as Figure 3. *Wind* and ACE were separated by 141 R_E along the *y*-direction.

Based on these three examples as well as the general statistics, we want to emphasize that for MEs, any difference in measurements between ACE and *Wind* is of short duration and typically associated with "dynamic" time shifting which may be associated with non-radial or non-uniform propagation of the ME. Additionally, the wake of MEs, while it contains magnetic fields of large amplitudes, appears to have a smaller coherence length than the ME. This should be confirmed in a follow-up study. Overall, there are no periods longer than 10 min with different signs of B_z at the two spacecraft unless B_z fluctuates around ±1 nT and the time series from both spacecraft are visually not distinguishable when plotted over the duration of a ME, that is, one day for mesoscales of 0.05–0.35° (20–140 R_E). This is consistent with their large-scale nature.

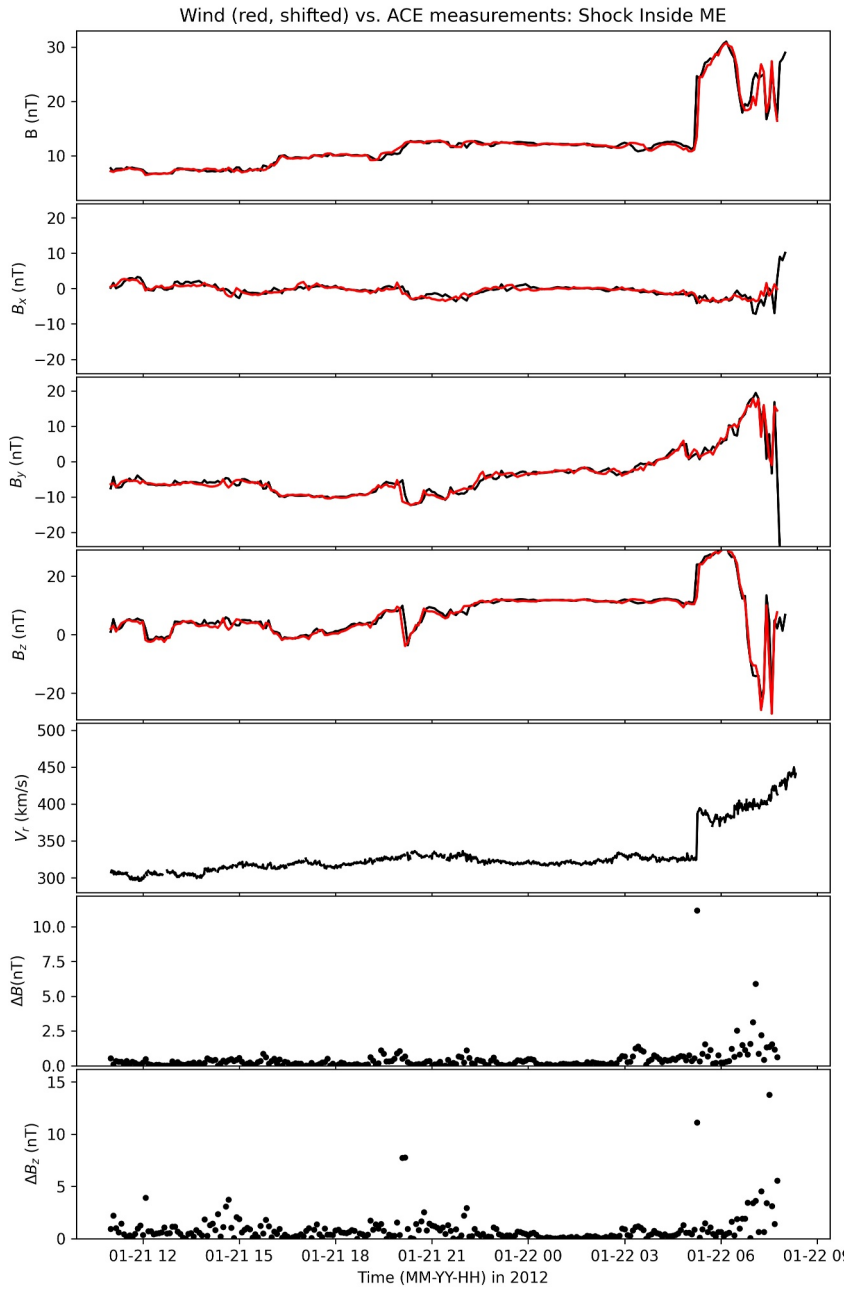

Figure 5. Time-shifted *Wind* (red) versus ACE (black) measurements for the 2012 January 21 coronal mass ejection and shock inside magnetic ejecta in the same format as Figure 3. *Wind* and ACE were separated by 75 R_E along the *y*-direction.

3.4. Effect of Moderate Angular Separations

In Lugaz, Zhuang, et al. (2024), the authors presented single and multi-spacecraft measurements of CMEs for separations of 20–60° taking advantage of the proximity of STEREO-A to the Sun-Earth line and L1 monitors in 2022–2023. The few multi-spacecraft events had significant differences in the duration and properties of the MEs, which make an analysis of the RMSE not fully appropriate. At intermediate separations of ∼2–10°, MEs tend to show visual similarities between two-spacecraft measurements, but relatively large differences in the medium-scale structures. An example of the analysis of such events can be found in Weiss et al. (2024) and other analyses are ongoing (e.g., see Weiler et al., 2024).

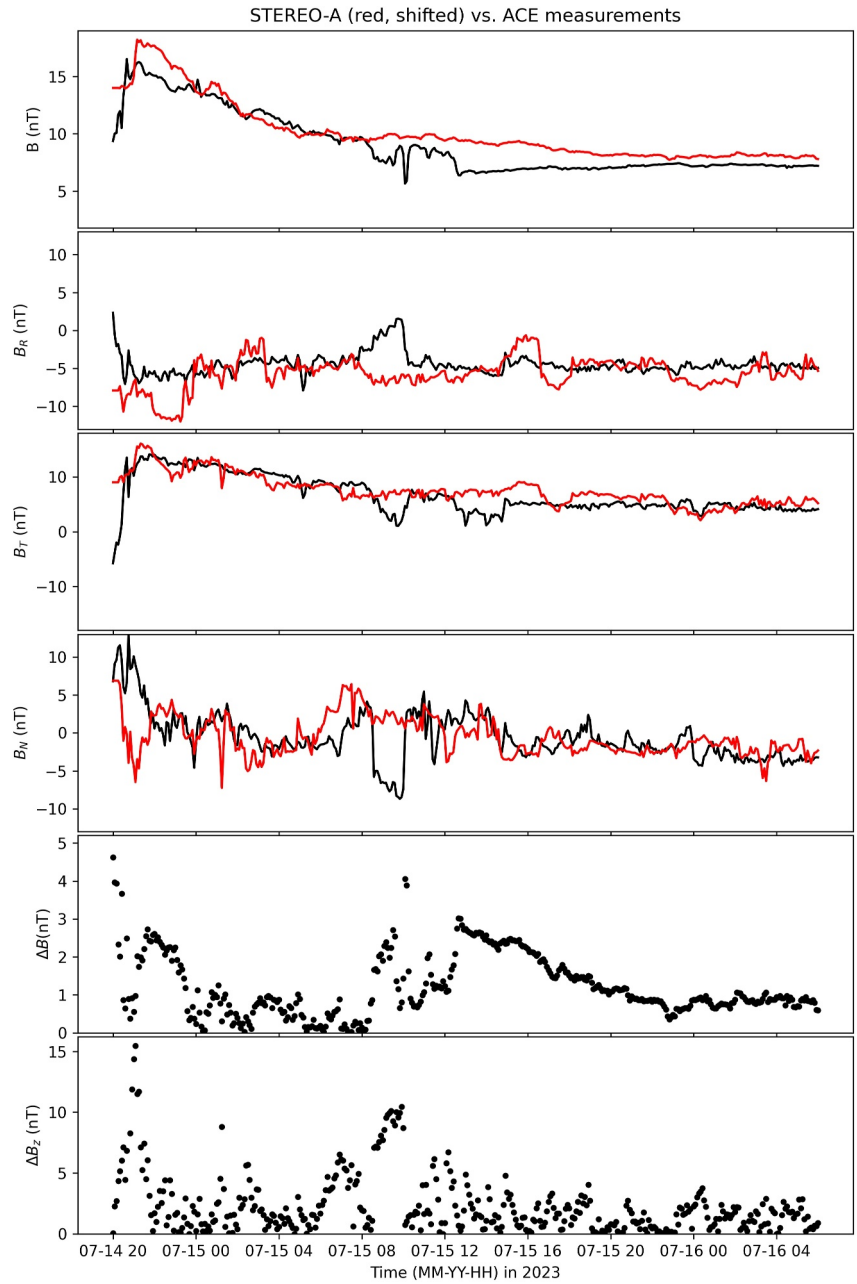

Figure 6. Time-shifted STEREO-A (red) versus ACE (black) measurements for the 2023 July 14 coronal mass ejection in the same format as Figure 3, except for the exclusion of the speed and the components being in *RTN* coordinates. STEREO-A and ACE were separated by 2.75° (∼1,100 R_E) along the *T*-direction.

In Figure 6, we present a similar analysis as that presented in the previous section but for ACE and STEREO-A measurements of the 2023 July 14–16 CME, when STEREO-A was 0.049 au upstream of L1 and 2.75° east of the Sun-Earth line. This corresponds to $\sim 7.1 \times 10^6$ km or about 1,100 R_E. The time shift that maximizes the correlation of B is 406 min (6 hr and 46 min), which would correspond to a radial propagation of about 300 km s^{-1}. The speed at the front of the ME was 400–430 km s^{-1}, faster than the speed derived assuming radial propagation and the best time shift, suggesting the presence of effects other than radial propagation. Investigating these effects are beyond the scope of this manuscript but are discussed briefly in the next section. The total magnetic field remains relatively well correlated with a correlation coefficient of about 0.924 inside the ME. The RMSE for B is 1.46 nT and it is 3.49 nT for B_z. Because B_z fluctuates around 0, there are 81 datapoints for which B_z has opposite

sign at ACE and STEREO-A and B_z is greater than 1 nT. The longest time period when this occurs is 90-min long starting at 8:35 UT for ACE. It corresponds to a period when B_z is negative around −6 nT at ACE and positive around +2 nT at STEREO-A. This period is about 2×10^6 km (~0.014 au) in size based on the speed of 380 km s^{-1}. This represents a mesoscale structure within the ME. As it occurs in the middle of the event, we consider it more likely that it represents an intrinsic non-uniform feature of the ME rather than the result of the interaction of the ME with the non-uniform solar wind. Overall, this shows that the RMSE between two spacecraft increases for increasing angular separation but remains "only" about 3 times larger than the typical RMSE between ACE and *Wind* for a separation of 2.75°. Some mesoscale differences also appear at these separations.

4. Evolution of CMEs and Shocks Over Moderate (0.03–0.25 AU) Radial Distances

The previous example highlights the difficulty of analyzing multi-spacecraft measurements when there are both a small angular separation (<3°) and a small separation in heliocentric distance (~0.05 au). The differences shown in Figure 6 may be due to the change of the ME properties with time (or heliocentric distance) or to the variations of the ME properties with longitude. For example, the average magnetic field in the ME is 10.1 nT at STEREO-A and 9.06 nT at ACE. This decrease of 10% over less than 0.05 au would correspond to the magnetic field decreasing with the heliocentric distance, r as $r^{-2.2}$, which is relatively steep as compared to the range of $r^{-1.6 \pm 0.3}$ obtained in past studies (Davies, Forsyth, et al., 2021; Winslow et al., 2015). It is, however, possible that this is due to the angular separation between the spacecraft since the magnetic field components have significant variations, which is hard to understand purely from propagation effects.

Laker et al. (2024) successfully hindcasted the arrival time of two CME events before they reached Earth using Solar Orbiter data from 0.44 to 0.48 au, that is, considerably further away from Earth than the other events discussed in this paper. We discuss two other examples from recently published work. In Davies, Möstl, et al. (2021), the authors analyzed measurements of a CME measured in 2020 April 19–20 at Solar Orbiter at 0.81 au and *Wind* at 1.0 au as they were separated by about 4.1° longitudinally as well as BepiColombo at 1.0 au and separated from *Wind* by 1.4° in longitude. The authors found a decrease of the average magnetic field as $r^{-1.1}$ between Solar Orbiter and *Wind*, which is significantly smaller compared to the one just discussed in Figure 6. This low exponent indicating a small expansion rate was attributed to this CME being sandwiched between very slow solar wind in the front and a high speed-stream at the back.

This kind of variability can have significant effects on the accuracy of the forecasts from upstream monitors. A sub-L1 monitor at 0.8 au measuring a ME with a mean magnetic field of 20 nT would forecast a ME with a mean magnetic field of 12.2 nT at 1 au assuming a decreasing as $r^{-2.2}$ but would forecast one of 15.6 nT assuming a decrease as $r^{-1.1}$. Whether potential errors of this magnitude (as much as 25%) are acceptable for forecasting agencies is not known at this time. Models that use power laws for the CME magnetic field evolution with distance such as 3DCORE would need to change the power law exponent according to the ambient wind conditions in order to forecast the total field magnitude with high accuracy, which is the type of research-to-operation and operation-to-research that requires further data. There were also significant differences in the measurements at *Wind* and BepiColombo for a period of 3.5–6 hr ahead of what Davies, Möstl, et al. (2021) referred to as the unperturbed magnetic flux rope. Farrugia et al. (2023) analyzed this "upstream" period (which is within the ME) and found that a combination of front erosion and internal reconnection within this region resulted in the differences measured at *Wind* and Solar Orbiter. However, the difference between *Wind* and BepiColombo may indicate that some of these differences are not evolutionary but spatial.

Another example was published in Regnault et al. (2024) for a CME measured by Solar Orbiter and L1 in 2021 November 3–5 when they were separated by 0.13 au in heliocentric distance and 2.2° in angle. The shock arrived only 5.5 hr earlier at Solar Orbiter than at *Wind*, which would correspond to a propagation speed of about 980 km s^{-1}. In fact, the shock speed and ME front speed were less than 800 km s^{-1}. This shows that the propagation was either not radial, or strongly affected by the 2° in angular separations or a combination of both. As discussed in Regnault et al. (2024), forecasting the arrival time of the shock at L1 using Solar Orbiter data would result in an error of 2.5 hr for a lead time of 5.5 hr or a relative error of more than 50%. That article also outlined significant differences in the magnetic field components inside the ME at the two spacecraft which may be due partially to temporal evolution in the 5.5 hr between the two measurements but more likely to spatial differences within the CME.

5. Discussion: Impact on Sub-L1 Operational Missions

In the previous sections, we highlighted several main points, first about the effect of angular separations between two spacecraft: (a) very small separations as compared to the CME size, of the order of 0.3°, do not appear to matter significantly to forecast ME properties (but they may matter for the forecast of shock and sheath properties), (b) moderate angular separations, of the order of a few degrees, can result in significant differences in part of the CMEs measured at two spacecraft but globally the measurements are still highly correlated, (c) starting at around 15° separation, two spacecraft are likely to not even measure the same CME. In addition, in those past studies, the two spacecraft are often separated in heliocentric distance as well as angularly. With only two spacecraft, it is impossible to distinguish between evolutionary and spatial variations. The event-to-event variability regarding the decrease of the magnetic field with distance appears large and could significantly affect the accuracy of sub-L1 monitors taken at heliocentric distances of 0.8 au or less. We next turn our attention of the consequence of these findings on the various types of sub-L1 monitors previously proposed.

5.1. Potential Orbits of Sub-L1 Monitors

Numerous orbits are possible for sub-L1 monitors and they can be classified broadly into the following categories: (a) "stationary" orbits near the Sun-Earth line with solar sails (Akhavan-Tafti et al., 2023; Eastwood et al., 2015; West, 1996), (b) heliocentric orbits, including drifters such as STEREO (Kaiser et al., 2008), the CUSP CubeSat (Desai et al., 2019) or the InterMeso mission concept (Allen et al., 2022) and distant retrograde orbits (DROs: Henon, 1969; St. Cyr et al., 2000), (c) planetary-like orbits (Ritter et al., 2015). While solar sail technology has progressed over the past two decades, a realistic sub-L1 monitor with solar sail technology would currently be limited to about 0.95 au, although high-TRL systems would be limited to about 0.97–0.98 au (see discussion in Akhavan-Tafti et al., 2023).

Drifters with a heliocentric distance of 0.95 au would require new platforms to be sent every 6–12 months based on a drift rate of ∼20° per year to stay within 10–20° of the Sun-Earth line. Spacecraft on a Sun-Earth DRO can reach up to 0.9 au while being within ±12° from the Sun-Earth line. The maximum separation with Earth along the GSE y axis is always twice that along the x axis (see Henon, 1969). As such, reaching up to 0.8 au means that the orbit reaches as far as ±24° from the Sun-Earth line. Four spacecraft are needed, as proposed for the Space Weather Diamond of St. Cyr et al. (2000) to ensure that one spacecraft is always upstream of L1 and always within ±6° of the Sun-Earth line, for a DRO reaching 0.9 au. A larger number of spacecraft would be needed to ensure that a mission reaching farther sunward remains within a small angular separation with the Sun-Earth line. Lastly, 6–36 satellites on a Venus-like (∼0.72 au) orbit would be needed to ensure that one spacecraft is always within ±5–30° from the Sun-Earth line. An example of a such a mission concept is that from Ritter et al. (2015).

5.2. Required Accuracy: Knowledge Gap

While a desired lead time of 6–24 hr for CME arrival time is relatively well documented (Vourlidas et al., 2023), the required accuracy has not been well appreciated. This raises one need for space weather research on sub-L1 measurements before operations, namely the determination of the accuracy of forecasting using sub-L1 monitors and the determination of whether they provide actionable forecasts.

It might be tempting to conclude from the investigations highlighted here that sub-L1 monitors should be located as close as possible to the Sun-Earth line so as to maximize the accuracy of the forecasts. However, a number of well known facts makes this suggestion impractical, as discussed for L1 monitors by Borovsky (2018). First, the Earth motion is about 1° per day, so a monitor at 0.9 au measuring a CME 6–12 hr before impact would need to be placed 0.25–0.5° west of the Sun-Earth line to measure the solar wind which is radially propagating toward Earth (this is the so-called solar wind aberration). Differences become obviously larger the farther upstream the sub-L1 monitor is. Second, the solar wind is not actually propagating radially, and Borovsky (2018) reports a median of 3.5° with a standard deviation of about 2.5° away from aberration-corrected radial direction, without a preferred direction. Al-Haddad et al. (2022) investigated non-radial flows and found that extreme values of non-radial flows (beyond 12° away from radial) are preferentially associated with SIRs and CME sheath regions. Non-radial flows within MEs were found to be frequent but weaker with typical angles around 4°. This indicates that separations of up to 5° from the Sun-Earth line may be sometimes optimal to forecast CME properties from sub-L1 monitors. This also indicates that a fixed location with respect to the Sun-Earth line is unlikely to be optimal for a majority of CMEs, and therefore a small constellation, associated with data assimilation and further research-to-operations

studies may be the optimal solution. The results presented here show that sub-L1 measurements within ∼12° of the Sun-Earth line may provide actionable forecasts for most CMEs impacting Earth, whereas measurements beyond that range may result in numerous false positives and misses. Based on this, it appears that any sub-L1 mission remaining within ∼12° of the Sun-Earth line could prove useful for space weather forecasting.

6. Recommendations

In conclusion, we make the following recommendations:

- A research-focused sub-L1 mission is needed to investigate (a) how CME properties vary as they propagate from upstream of L1 to L1, (b) how CME properties vary for moderate angular separations (0.5–10°), and (c) what location(s) with respect to Earth are the most adequate ones for a future operational sub-L1 mission.
- Such a mission should be restricted to longitudinal separations of $\lesssim$15° from the Sun-Earth line to ensure that the majority of CMEs impacting the sub-L1 platform also impact L1. In an operational setting, this requires four spacecraft on a DRO but as many as 12 for spacecraft on a planetary orbit.
- Such a mission should have a beacon mode allowing for real-time data to be evaluated in real forecasting settings. The design decisions for such a beacon mode should be made early during the preliminary design of the missions. This could be done through a space weather enhancement opportunity, similar to science enhancement opportunity and would ensure that any design decision related to these hybrid approaches is incorporated early in the mission profile and that any agreement between research and operational agencies occur well ahead of the final design of the mission.
- For large geomagnetic storms driven by magnetic clouds and ME, L1 and sub-L1 platforms may be adequate since the variability of ME on scales of less than 0.5° is small and may remain small even for a few degrees.

Data Availability Statement

All in situ measurements used in this research are publicly available through NASA SPDF (https://spdf.gsfc.nasa.gov). The *Wind*, ACE and STEREO data was downloaded from CDAWeb (https://cdaweb.gsfc.nasa.gov). OMNI data was downloaded from omniweb (https://omniweb.gsfc.nasa.gov).

Acknowledgments
N. L., N. A., B. Z. R. M. W. and C. J. F. were funded by 80NSSC21K0463, 80NSSC22K0349, 80NSSC20K0700, 80NSSC23K1057, AGS-1954983, and AGS-2301382. C. M., E. E. D. and E. W. acknowledge funding by the European Union (ERC, HELIO4CAST, 101042188). Views and opinions expressed are however those of the author(s) only and do not necessarily reflect those of the European Union or the European Research Council Executive Agency. Neither the European Union nor the granting authority can be held responsible for them.

References

Akhavan-Tafti, M., Johnson, L., Sood, R., Slavin, J. A., Pulkkinen, T., Lepri, S., et al. (2023). Space weather investigation Frontier (SWIFT). *Frontiers in Astronomy and Space Sciences*, *10*, 1185603. https://doi.org/10.3389/fspas.2023.1185603

Ala-Lahti, M., Ruohotie, J., Good, S., Kilpua, E. K. J., & Lugaz, N. (2020). Spatial coherence of interplanetary coronal mass ejection sheaths at 1 AU. *Journal of Geophysical Research: Space Physics*, *125*(9), e2020JA028002. https://doi.org/10.1029/2020JA028002

Al-Haddad, N., Galvin, A. B., Lugaz, N., Farrugia, C. J., & Yu, W. (2022). Investigating the cross sections of coronal mass ejections through the study of nonradial flows with STEREO/PLASTIC. *The Astrophysical Journal*, *927*(1), 68. https://doi.org/10.3847/1538-4357/ac32e1

Allen, R. C., Smith, E. J., Anderson, B. J., Borovsky, J. E., Ho, G. C., Jian, L., et al. (2022). Interplanetary mesoscale observatory (InterMeso): A mission to untangle dynamic mesoscale structures throughout the heliosphere. *Frontiers in Astronomy and Space Sciences*, *9*, 1002273. https://doi.org/10.3389/fspas.2022.1002273

Bailey, R. L., Möstl, C., Reiss, M. A., Weiss, A. J., Amerstorfer, U. V., Amerstorfer, T., et al. (2020). Prediction of Dst during solar minimum using in situ measurements at L5. *Space Weather*, *18*(5), e2019SW002424. https://doi.org/10.1029/2019SW002424

Borovsky, J. E. (2018). The spatial structure of the oncoming solar wind at Earth and the shortcomings of a solar-wind monitor at L1. *Journal of Atmospheric and Solar-Terrestrial Physics*, *177*, 2–11. https://doi.org/10.1016/j.jastp.2017.03.014

Burton, R. K., McPherron, R. L., & Russell, C. T. (1975). An empirical relationship between interplanetary conditions and Dst. *Journal of Geophysical Research*, *80*(31), 4204–4214. https://doi.org/10.1029/JA080i031p04204

Chi, Y., Shen, C., Scott, C., Xu, M., Owens, M., Wang, Y., & Lockwood, M. (2022). Predictive capabilities of corotating interaction regions using STEREO and wind in-situ observations. *Space Weather*, *20*(7), e2022SW003112. https://doi.org/10.1029/2022SW003112

Davies, E. E., Forsyth, R. J., Winslow, R. M., Möstl, C., & Lugaz, N. (2021a). A Catalog of Interplanetary Coronal Mass Ejections Observed by Juno between 1 and 5.4 au. *The Astrophysical Journal*, *923*(2), 136. https://doi.org/10.3847/1538-4357/ac2ccb

Davies, E. E., Möstl, C., Owens, M. J., Weiss, A. J., Amerstorfer, T., Hinterreiter, J., et al. (2021). In situ multi-spacecraft and remote imaging observations of the first CME detected by Solar Orbiter and BepiColombo. *Astronomy and Astrophysics*, *656*, A2. https://doi.org/10.1051/0004-6361/202040113

Desai, M. I., Allegrini, F., Ebert, R. W., Ogasawara, K., Epperly, M. E., George, D. E., et al. (2019). The cubesat mission to study solar particles. *IEEE Aerospace and Electronic Systems Magazine*, *34*(4), 16–28. https://doi.org/10.1109/MAES.2019.2917802

Eastwood, J. P., Brown, P., Magnes, W., Carr, C. M., Agu, M., Baughen, R., et al. (2024). The Vigil magnetometer for operational space weather services from the Sun-Earth L5 point. *Space Weather*, *22*(6), e2024SW003867. https://doi.org/10.1029/2024SW003867

Eastwood, J. P., Kataria, D. O., McInnes, C. R., Barnes, N. C., & Mulligan, P. (2015). Sunjammer. *Weather*, *70*(1), 27–30. https://doi.org/10.1002/wea.2438

Farquhar, R. W. (2001). The Flight of ISEE-3/ICE: Origins, mission history, and a legacy. *Journal of the Astronautical Sciences*, *49*(1), 23–73. https://doi.org/10.1007/BF03546336

Farrugia, C. J., Vasquez, B. J., Lugaz, N., Al-Haddad, N. A., Richardson, I. G., Davies, E. E., et al. (2023). How magnetic reconnection may affect the coherence of interplanetary coronal mass ejections. *The Astrophysical Journal*, *953*(1), 15. https://doi.org/10.3847/1538-4357/acdcf7

Good, S. W., & Forsyth, R. J. (2016). Interplanetary coronal mass ejections observed by MESSENGER and Venus express. *Solar Physics*, *291*(1), 239–263. https://doi.org/10.1007/s11207-015-0828-3

Henon, M. (1969). Numerical exploration of the restricted problem. *Astronomy and Astrophysics*, *1*, 223–238.

Howard, T. A., & Harrison, R. A. (2013). Stealth coronal mass ejections: A perspective. *Solar Physics*, *285*(1–2), 269–280. https://doi.org/10.1007/s11207-012-0217-0

Jian, L. K., Russell, C. T., Luhmann, J. G., & Galvin, A. B. (2018). STEREO observations of interplanetary coronal mass ejections in 2007 – 2016. *The Astrophysical Journal*, *855*(2), 114. https://doi.org/10.3847/1538-4357/aab189

Kaiser, M. L., Kucera, T. A., Davila, J. M., St. Cyr, O. C., Guhathakurta, M., & Christian, E. (2008). The STEREO mission: An introduction. *Space Science Reviews*, *136*(1–4), 5–16. https://doi.org/10.1007/s11214-007-9277-0

Kay, C., Mays, M. L., & Collado-Vega, Y. M. (2022). OSPREI: A coupled approach to modeling CME-driven space weather with automatically generated, user-friendly outputs. *Space Weather*, *20*(4), e2021SW002914. https://doi.org/10.1029/2021SW002914

Kay, C., Opher, M., & Evans, R. M. (2013). Forecasting a coronal mass ejection's altered trajectory: ForeCAT. *The Astrophysical Journal*, *775*(1), 5. https://doi.org/10.1088/0004-637X/775/1/5

Kay, C., Palmerio, E., Riley, P., Mays, M. L., Nieves-Chinchilla, T., Romano, M., et al. (2024). Updating measures of CME arrival time errors. *Space Weather*, *22*(7), e2024SW003951. https://doi.org/10.1029/2024SW003951

Kilpua, E. K. J., Lee, C. O., Luhmann, J. G., & Li, Y. (2011). Interplanetary coronal mass ejections in the near-Earth solar wind during the minimum periods following solar cycles 22 and 23. *Annals of Geophysics*, *29*(8), 1455–1467. https://doi.org/10.5194/angeo-29-1455-2011

Kilpua, E. K. J., Lumme, E., Andreeova, K., Isavnin, A., & Koskinen, H. E. J. (2015). Properties and drivers of fast interplanetary shocks near the orbit of the Earth (1995-2013). *Journal of Geophysical Research: Space Physics*, *120*(6), 4112–4125. https://doi.org/10.1002/2015JA021138

Koval, A., & Szabo, A. (2010). Multispacecraft observations of interplanetary shock shapes on the scales of the Earth's magnetosphere. *Journal of Geophysical Research*, *115*(A12), A12105. https://doi.org/10.1029/2010JA015373

Kubicka, M., Möstl, C., Amerstorfer, T., Boakes, P. D., Feng, L., Eastwood, J. P., & Törmänen, O. (2016). Prediction of geomagnetic storm strength from inner heliospheric in situ observations. *The Astrophysical Journal*, *833*(2), 255. https://doi.org/10.3847/1538-4357/833/2/255

Laker, R., Horbury, T. S., O'Brien, H., Fauchon-Jones, E. J., Angelini, V., Fargette, N., et al. (2024). Using solar orbiter as an upstream solar wind monitor for real time space weather predictions. *Space Weather*, *22*(2), e2023SW003628. https://doi.org/10.1029/2023SW003628

Leitner, M., Farrugia, C. J., MöStl, C., Ogilvie, K. W., Galvin, A. B., Schwenn, R., & Biernat, H. K. (2007). Consequences of the force-free model of magnetic clouds for their heliospheric evolution. *Journal of Geophysical Research*, *112*(A6), A06113. https://doi.org/10.1029/2006JA011940

Lindsay, G. M., Russell, C. T., & Luhmann, J. G. (1999). Predictability of Dst index based upon solar wind conditions monitored inside 1 AU. *Journal of Geophysical Research*, *104*(A5), 10335–10344. https://doi.org/10.1029/1999JA900010

Liu, J., Ye, Y., Shen, C., Wang, Y., & Erdélyi, R. (2018). A new tool for CME arrival time prediction using machine learning algorithms: CAT-PUMA. *The Astrophysical Journal*, *855*(2), 109. https://doi.org/10.3847/1538-4357/aaae69

Liu, Y. D., Hu, H., Zhao, X., Chen, C., & Wang, R. (2024). A pileup of coronal mass ejections produced the largest geomagnetic storm in two decades. *The Astrophysical Journal Letters*, *974*(1), L8. https://doi.org/10.3847/2041-8213/ad7ba4

Liu, Y. D., Luhmann, J. G., Kajdič, P., Kilpua, E. K. J., Lugaz, N., Nitta, N. V., et al. (2014). Observations of an extreme storm in interplanetary space caused by successive coronal mass ejections. *Nature Communications*, *5*(1), 3481. https://doi.org/10.1038/ncomms4481

Loto'aniu, P. T. M., Romich, K., Rowland, W., Codrescu, S., Biesecker, D., Johnson, J., et al. (2022). Validation of the DSCOVR spacecraft mission space weather solar wind products. *Space Weather*, *20*(10), e2022SW003085. https://doi.org/10.1029/2022SW003085

Lugaz, N., Farrugia, C. J., Smith, C. W., & Paulson, K. (2015). Shocks inside CMEs: A survey of properties from 1997 to 2006. *Journal of Geophysical Research: Space Physics*, *120*(4), 2409–2427. https://doi.org/10.1002/2014JA020848

Lugaz, N., Farrugia, C. J., Winslow, R. M., Al-Haddad, N., Galvin, A. B., Nieves-Chinchilla, T., et al. (2018). On the Spatial Coherence of Magnetic Ejecta: Measurements of Coronal Mass Ejections by Multiple Spacecraft Longitudinally Separated by 0.01 au. *The Astrophysical Journal Letters*, *864*(1), L7. https://doi.org/10.3847/2041-8213/aad9f4

Lugaz, N., Farrugia, C. J., Winslow, R. M., Al-Haddad, N., Kilpua, E. K. J., & Riley, P. (2016). Factors affecting the geoeffectiveness of shocks and sheaths at 1 AU. *Journal of Geophysical Research: Space Physics*, *121*(A10), 10. https://doi.org/10.1002/2016JA023100

Lugaz, N., Lee, C. O., Jian, L. K., Allen, R., Al-Haddad, N., Winslow, R. M., et al. (2024). The need for near-Earth multi-spacecraft heliospheric measurements and an explorer mission to investigate interplanetary structures and transients in the near-Earth heliosphere. *Space Science Reviews*, *220*, 73. https://doi.org/10.1007/s11214-024-01108-8

Lugaz, N., Zhuang, B., Scolini, C., Al-Haddad, N., Farrugia, C. J., Winslow, R. M., et al. (2024). The Width of Magnetic Ejecta Measured near 1 au: Lessons from STEREO-A Measurements in 2021–2022. *The Astrophysical Journal*, *962*(2), 193. https://doi.org/10.3847/1538-4357/ad17b9

McComas, D. J., Christian, E. R., Schwadron, N. A., Fox, N., Westlake, J., Allegrini, F., et al. (2018). Interstellar mapping and acceleration probe (IMAP): A new NASA mission. *Space Science Reviews*, *214*(8), 116. https://doi.org/10.1007/s11214-018-0550-1

Morley, S. K. (2020). Challenges and opportunities in magnetospheric space weather prediction. *Space Weather*, *18*(3), e02108. https://doi.org/10.1029/2018SW002108

Morley, S. K., Welling, D. T., & Woodroffe, J. R. (2018). Perturbed input ensemble modeling with the space weather modeling framework. *Space Weather*, *16*(9), 1330–1347. https://doi.org/10.1029/2018SW002000

Möstl, C., Amerstorfer, T., Palmerio, E., Isavnin, A., Farrugia, C. J., Lowder, C., et al. (2018). Forward modeling of coronal mass ejection flux ropes in the inner heliosphere with 3DCORE. *Space Weather*, *16*(3), 216–229. https://doi.org/10.1002/2017SW001735

Möstl, C., Weiss, A. J., Bailey, R. L., Reiss, M. A., Amerstorfer, T., Hinterreiter, J., et al. (2020). Prediction of the in situ coronal mass ejection rate for solar cycle 25: Implications for Parker solar probe in situ observations. *The Astrophysical Journal*, *903*(2), 92. https://doi.org/10.3847/1538-4357/abb9a1

Nieves-Chinchilla, T., Vourlidas, A., Raymond, J. C., Linton, M. G., Al-haddad, N., Savani, N. P., et al. (2018). Understanding the internal magnetic field configurations of ICMEs using more than 20 years of wind observations. *Solar Physics*, *293*(2), 25. https://doi.org/10.1007/s11207-018-1247-z

Nitta, N. V., Mulligan, T., Kilpua, E. K. J., Lynch, B. J., Mierla, M., O'Kane, J., et al. (2021). Understanding the origins of problem geomagnetic storms associated with "stealth" coronal mass ejections. *Space Science Reviews*, *217*(8), 82. https://doi.org/10.1007/s11214-021-00857-0

O'Brien, T. P., & McPherron, R. L. (2000). An empirical phase space analysis of ring current dynamics: Solar wind control of injection and decay. *Journal of Geophysical Research*, *105*(A4), 7707–7720. https://doi.org/10.1029/1998JA000437

Odstrcil, D., & Pizzo, V. J. (2009). Numerical heliospheric simulations as assisting tool for interpretation of observations by STEREO heliospheric imagers. *Solar Physics*, *259*(1–2), 297–309. https://doi.org/10.1007/s11207-009-9449-z

Odstrcil, D., Vandas, M., Pizzo, V. J., & MacNeice, P. (2003). Numerical simulation of interacting magnetic flux ropes. In M. Velli, R. Bruno, F. Malara, & B. Bucci (Eds.), *Solar wind ten* (Vol. 679, pp. 699–702). https://doi.org/10.1063/1.1618690

Palmerio, E., Kilpua, E. K. J., Möstl, C., Bothmer, V., James, A. W., Green, L. M., et al. (2018). Coronal magnetic structure of Earthbound CMEs and in situ comparison. *Space Weather*, *16*(5), 442–460. https://doi.org/10.1002/2017SW001767

Poedts, S., Lani, A., Scolini, C., Verbeke, C., Wijsen, N., Lapenta, G., et al. (2020). EUropean heliospheric FORecasting information asset 2.0. *Journal of Space Weather and Space Climate*, *10*, 57. https://doi.org/10.1051/swsc/2020055

Pomoell, J., & Poedts, S. (2018). EUHFORIA: European heliospheric forecasting information asset. *Journal of Space Weather and Space Climate*, *8*, A35. https://doi.org/10.1051/swsc/2018020

Regnault, F., Al-Haddad, N., Lugaz, N., Farrugia, C. J., Yu, W., Zhuang, B., & Davies, E. E. (2024). Discrepancies in the Properties of a Coronal Mass Ejection on Scales of 0.03 au as Revealed by Simultaneous Measurements at Solar Orbiter and Wind: The 2021 November 3–5 Event. *The Astrophysical Journal*, *962*(2), 190. https://doi.org/10.3847/1538-4357/ad1883

Regnault, F., Janvier, M., Démoulin, P., Auchère, F., Strugarek, A., Dasso, S., & Noûs, C. (2020). 20 Years of ACE data: How superposed epoch analyses reveal generic features in interplanetary CME profiles. *Journal of Geophysical Research: Space Physics*, *125*(11), e28150. https://doi.org/10.1029/2020JA028150

Richardson, I. G., & Cane, H. V. (2010). Near-Earth interplanetary coronal mass ejections during solar cycle 23 (1996 - 2009): Catalog and summary of properties. *Solar Physics*, *264*(1), 189–237. https://doi.org/10.1007/s11207-010-9568-6

Riley, P., Mays, M. L., Andries, J., Amerstorfer, T., Biesecker, D., Delouille, V., et al. (2018). Forecasting the arrival time of coronal mass ejections: Analysis of the CCMC CME scoreboard. *Space Weather*, *16*(9), 1245–1260. https://doi.org/10.1029/2018SW001962

Ritter, B., Meskers, A. J. H., Miles, O., Rußwurm, M., Scully, S., Roldán, A., et al. (2015). A space weather information service based upon remote and in-situ measurements of coronal mass ejections heading for Earth. *Journal of Space Weather and Space Climate*, *5*, A3. https://doi.org/10.1051/swsc/2015006

Rüdisser, H. T., Weiss, A. J., Le Louëdec, J., Amerstorfer, U. V., Möstl, C., Davies, E. E., & Lammer, H. (2024). Understanding the effects of spacecraft trajectories through solar coronal mass ejection flux ropes using 3DCOREweb. arXiv e-prints, arXiv:2405.03271. *The Astrophysical Journal*, *973*(2), 150. https://doi.org/10.48550/arXiv.2405.03271

Salman, T. M., Lugaz, N., Winslow, R. M., Farrugia, C. J., Jian, L. K., & Galvin, A. B. (2021). Categorization of coronal mass ejection-driven sheath regions: Characteristics of STEREO events. *The Astrophysical Journal*, *921*(1), 57. https://doi.org/10.3847/1538-4357/ac11f3

Salman, T. M., Winslow, R. M., & Lugaz, N. (2020). Radial evolution of coronal mass ejections between MESSENGER, *Venus express*, STEREO, and L1: Catalog and analysis. *Journal of Geophysical Research*, *125*(1), e2019JA027084. https://doi.org/10.1029/2019JA027084

Sarkar, R., Srivastava, N., Gopalswamy, N., & Kilpua, E. (2024). Modeling the magnetic vectors of interplanetary coronal mass ejections at different heliocentric distances with INFROS. *The Astrophysical Journal - Supplement Series*, *273*(2), 36. https://doi.org/10.3847/1538-4365/ad5835

Savani, N. P., Vourlidas, A., Pulkkinen, A., Nieves-Chinchilla, T., Lavraud, B., & Owens, M. J. (2013). Tracking the momentum flux of a CME and quantifying its influence on geomagnetically induced currents at Earth. *Space Weather*, *11*(5), 245–261. https://doi.org/10.1002/swe.20038

Savani, N. P., Vourlidas, A., Szabo, A., Mays, M. L., Richardson, I. G., Thompson, B. J., et al. (2015). Predicting the magnetic vectors within coronal mass ejections arriving at Earth: 1. Initial architecture. *Space Weather*, *13*(6), 374–385. https://doi.org/10.1002/2015SW001171

St. Cyr, O. C., Plunkett, S. P., Michels, D. J., Paswaters, S. E., Koomen, M. J., Simnett, G. M., et al. (2000). Properties of coronal mass ejections: SOHO LASCO observations from January 1996 to June 1998. *Journal of Geophysical Research*, *105*, 18169–18186. https://doi.org/10.1029/1999JA000381

Stone, E. C., Frandsen, A. M., Mewaldt, R. A., Christian, E. R., Margolies, D., Ormes, J. F., & Snow, F. (1998). The advanced composition explorer. *Space Science Reviews*, *86*(1/4), 1–22. https://doi.org/10.1023/A:1005082526237

Talaat, E. R. (2023). NOAA's space weather next (SW next) program. In *AGU fall meeting abstracts* (Vol. 2023, p. SH32C-08).

Tóth, G., van der Holst, B., Sokolov, I. V., de Zeeuw, D. L., Gombosi, T. I., Fang, F., et al. (2012). Adaptive numerical algorithms in space weather modeling. *Journal of Computational Physics*, *231*(3), 870–903. https://doi.org/10.1016/j.jcp.2011.02.006

Vourlidas, A., Turner, D., Biesecker, D., Coster, A., Engell, A., Ho, G., et al. (2023). The NASA space weather science and observation gap analysis. *Advances in Space Research*. in press. https://doi.org/10.1016/j.asr.2023.06.046

Walsh, B. M., Bhakyapaibul, T., & Zou, Y. (2019). Quantifying the uncertainty of using solar wind measurements for geospace inputs. *Journal of Geophysical Research: Space Physics*, *124*(5), 3291–3302. https://doi.org/10.1029/2019JA026507

Wang, Y., Shen, C., Wang, S., & Ye, P. (2004). Deflection of coronal mass ejection in the interplanetary medium. *Solar Physics*, *222*(2), 329–343. https://doi.org/10.1023/B:SOLA.0000043576.21942.aa

Wang, Y., Xue, X., Shen, C., Ye, P., Wang, S., & Zhang, J. (2006). Impact of major coronal mass ejections on geospace during 2005 September 7-13. *The Astrophysical Journal*, *646*(1), 625–633. https://doi.org/10.1086/504676

Weiler, E., Möstl, C., Davies, E. E., Veronig, A., Amerstorfer, U. V., Amerstorfer, T., et al. (2024). First observations of a geomagnetic superstorm with a sub-L1 monitor. arXiv e-prints, arXiv:2411.12490. https://doi.org/10.48550/arXiv.2411.12490

Weiss, A. J., Möstl, C., Davies, E. E., Amerstorfer, T., Bauer, M., Hinterreiter, J., et al. (2021). Multi-point analysis of coronal mass ejection flux ropes using combined data from Solar Orbiter, BepiColombo, and Wind. *Astronomy and Astrophysics*, *656*, A13. https://doi.org/10.1051/0004-6361/202140919

Weiss, A. J., Nieves-Chinchilla, T., & Möstl, C. (2024). Distorted magnetic flux ropes within interplanetary coronal mass ejections. *The Astrophysical Journal*, *975*(2), 169. https://doi.org/10.3847/1538-4357/ad7940

West, J. L. (1996). NOAA/DoD/NASA geostorm warning mission. In *Jpl d-13986*.

Wilson, I., Lynn, B., Brosius, A. L., Gopalswamy, N., Nieves-Chinchilla, T., Szabo, A., et al. (2021). A quarter century of wind spacecraft discoveries. *Review of Geophysics*, *59*(2), e2020RG000714. https://doi.org/10.1029/2020RG000714

Winslow, R. M., Lugaz, N., Philpott, L. C., Schwadron, N. A., Farrugia, C. J., Anderson, B. J., & Smith, C. W. (2015). Interplanetary coronal mass ejections from MESSENGER orbital observations at Mercury. *Journal of Geophysical Research: Space Physics*, *120*(8), 6101–6118. https://doi.org/10.1002/2015JA021200

Yang, Y., Liu, J., Feng, X., Chen, P., & Zhang, B. (2023). Prediction of the transit time of coronal mass ejections with an ensemble machine-learning method. *The Astrophysical Journal - Supplement Series*, *268*(2), 69. https://doi.org/10.3847/1538-4365/acf218

Zhuang, B., Wang, Y., Shen, C., Liu, S., Wang, J., Pan, Z., et al. (2017). The significance of the influence of the CME deflection in interplanetary space on the CME arrival at Earth. *The Astrophysical Journal*, *845*(2), 117. https://doi.org/10.3847/1538-4357/aa7fc0